Electric Power Systems Research 181 (2020) 106196

Contents lists available at ScienceDirect

Electric Power Systems Research

journal homepage: www.elsevier.com/locate/epsr

# Simulation and experimental comparative analysis of the DC-DC converter topologies for wind driven SEIG fed DC nanogrid

Saurabh Kumar[a], Vijayakumar K[b,*]

[a] Electrical Engineering Department, Malaviya National Institute of Technology (Govt. of India), Jaipur 302017, India
[b] Department of Electronics and Communication Engineering, Indian Institute of Information Technology Design and Manufacturing (IIITDM), Kancheepuram, India

ARTICLE INFO

*Keywords:*
DC nanogrid
DC-DC converter
Wind energy conversion system
SEIG
DBR

ABSTRACT

Wind energy conversion system (WECS) based DC nanogrid topology is proposed in this paper. The WECS topology is based on self-excited induction generator (SEIG) which is cost effective, and has rugged construction and combination of diode bridge rectifier (DBR) with DC-DC converter to implement the maximum power point tracking technique. The combination of diode DBR with DC-DC converter allows simple control structure due to one controllable switch as compared to complex control in the conventional controlled/semi-controlled rectifier with six controllable switches. Further, proposed DC nanogrid topology enhances the SEIG efficiency due to the reduction of harmonic injection on machine side from DBR implementation. The detailed harmonic spectrum analysis is carried out by developing the laboratory scale prototype of DBR based SEIG topology for WECS to justify the selection of DBR instead of the controlled rectifier. Further, to analyze the effect of different types DC-DC converter to make combination with the DBR. Afterwards, the dynamic performance of the proposed DC nanogrid topology is analyzed to understand the selection of the DC-DC converter with DBR for different DC grid voltage conditions.

## 1. Introduction

Electricity plays a vital role in energy supply, however, the electricity generation is the single largest source of $CO_2$ emission, which is more than 40% of $CO_2$ emission related to global energy. By the year 2030, global electricity demand is likely to double [1,2]. Hence, climate change mitigation and increasing energy demand motivates for the development of renewable energy resources. The renewable energy resources such as solar and wind energy are distributed in nature which favors the electricity generation and consumption on site. With technological advancement and regulatory changes, the concept of supplying the load locally has led to a concept of nanogrid. Thus, the development of renewable based nanogrid are gaining attention in recent past for providing environment-friendly, sustainable and economical electricity [3]. Further, the development of power electronics has transformed the load profile of end user as the modern appliances operate on DC supply [4]. Having this understanding, the concept of DC nanogrid has been proposed in the literature to elude multiple AC-DC conversion and vice-versa [5]. The DC distribution enables easy control, no issue of frequency, power angle, phase sequence, and power factor. Mashood et al. have proposed an optimized scalable solar based DC microgrid architecture for rural electrification with emphasis on the providing power for purposes beyond those related to subsistence-level living [6]. In Ref. [7], a converter topology is proposed for integrating hybrid energy storage in DC microgrid. However, the primary energy source considered is solar photovoltaic (SPV). There are substantial deployment of SPV based DC nanogrid considering that PV panels are DC power source, which has stimulated the implementation of smart grid in the bottom up manner [8]. With the advancement in power electronics and wind turbine technology, the small scale wind energy conversion system (WECS) could become a prominent source of renewable energy in DC nanogrid [9,10].

Scaling down the well developed technology for large scale WECS, for DC nanogrid application leads to costlier electricity generation. Wind generators and power electronic converters are the core of a WECS. The variable speed wind turbines are desired to extract the maximum power from the wind by incorporating maximum power point tracking (MPPT). Permanent magnet synchronous generator (PMSG), doubly fed induction generator (DFIG), wound rotor induction generator (WRIG) and SEIG are employed with variable wind speed turbines. DFIG is a slip ring induction generator which operates in both sub-synchronous and super-synchronous speeds providing a range of ± 30% of the rated speed for the MPPT operation. DFIG with a single inverter-battery system feeding isolated AC loads is proposed, as DFIG

* Corresponding author.
*E-mail address:* vijayakumar@iiitdm.ac.in (V. K).

https://doi.org/10.1016/j.epsr.2020.106196
Received 20 March 2019; Received in revised form 20 November 2019; Accepted 3 January 2020
Available online 11 January 2020
0378-7796/ 

supply constant frequency power at variable speed [11]. DFIG based system are suitable for medium and large scale WECS as DFIG based system employs reduced sized power electronic converters. WRIG with rotor resistance control based WECS is a simple system with single power electronic switch control. However, WRIG has limited speed range for MPPT and efficiency of the system reduces due to losses in resistances [12]. PMSG has high efficiency, yield, power to weight ratio and reliability, therefore a preferable option for variable speed operation. In literature, the PMSG has been proposed for large scale grid connected WECS [13]. Similarly in Ref. [14], an improved MPPT for PMSG based two stage WECS is proposed for large scale wind farms. The proposed MPPT technique is effective in terms of wind energy capture efficiency, reduced computation time and simple to implement. However, it is not suitable for varying wind speed and turbulence. Further, the PMSG is not viable for small scale WECS because of higher cost and difficulties in manufacturing. In recent days, induction machine has seen growth in uses as generator in WECS mainly for rural electrification. SEIG has numerous advantages, such as little maintenance, rugged and simple construction, and brushless operation, low cost and absence of external power supply to produce excitation. The comparison of various generator topologies on various parameter is presented in Table 1 [15–18].

Conventionally, SCIG is directly connected to grid without any power electronic converter that allows fixed speed operation resulting in poor efficiency. Additionally, the wind speed dynamics are transferred into electromechanical torque fluctuation resulting in mechanical stress on the system and swing oscillation. Further, voltage and frequency regulation is challenging task for such system [19,20]. In order to enhance the conversion efficiency, two speed topology (full rated and partially rated speed) consisting of two generator coupled to a single shaft or dual shaft using split gearbox. This type of system requires two generators which increases the weight of the system along with additional cost, and mechanical complexity [16]. Further, SCIG with a controlled rectifier which compensates the reactive power demand and coupled to grid using an inverter as shown in Fig. 1. The topology uses full capacity controlled rectifier which increases the number of power electronic switches, the complexity in control and cost. A simple topology of WECS consisting of SCIG connected parallel with capacitor banks also known as SEIG, to meet the reactive power demand is employed to supply the standalone loads is proposed in Ref. [21]. SEIG without any power electronic interface has poor voltage and frequency regulation, and efficiency. A SEIG based WECS for battery charging and DC power application is proposed. The problem with this topology is the additional firing circuit requirement, and power quality issue [22]. Further, a single stage SEIG based WECS topology for DC microgrid is proposed [9]. A semi controlled converter is connected between SEIG and DC bus for MPPT. The proposed system has three controllable switch which is less than single stage controlled rectifier based topology. Considering the above review of WECS topologies and generators, SEIG has rugged construction, little maintenance due to brushless operation and least cost. However, SEIG based WECS topologies either have large number of power electronic switches leading to complexity in control or has poor voltage and frequency regulation. However, the two stage PMSG based WECS has less number of power electronics switches and has simple control. It would be interesting to implement a two stage converter topology similar to PMSG based WECS for SEIG based DC nanogrid system. Therefore, in this paper, SEIG based WECS topology suitable for DC nanogrid is proposed, which consists of a SEIG supplying to a DBR followed by a DC-DC converter. The proposed topology has only one controlled power electronic switch which provides easy control and good power quality on the stator side due to reduced harmonics.

To enhance the efficiency and reliability of nanogrid, it is very important to extract the maximum power from renewable resources. Since, WECS does not operate at maximum power point by default, it is desirable to implement a MPPT technique for extracting the maximum power. Based on the power equation of wind turbine, numerous maximum power points tracking techniques have been proposed in the literature. In this regard the MPPT technique proposed mainly for large WECS consist of mechanical tracking of the turbine and by using converters. However, these conventional MPPT techniques make use of mechanical sensor making it costly. High cost eliminate the possibility of use of these MPPT technique for small scale WECS. In order to manage the cost, MPPT techniques based on the electrical parameter have been proposed in the literature. In AC nanogrid, the control strategy based on rectifier and inverter, the DC link is not maintained constant due to varying wind speed. Consequently, the modulation index of voltage source inverter has to be varied beyond 1 at low wind speeds which reduces the switching frequency which requires large sized filters. The machine side converter controller for SEIG should decouple the active and reactive power to generate the pulse width modulating signal to feed the driver circuit of the controllable switches. Also implementing MPPT on grid side inverter needs the mechanical speed sensor which reduces the MPPT accuracy and operational and maintenance cost increases. Therefore, MPPT algorithms which are based on the measured electrical quantities are gaining popularity and are implemented using the grid side converter. There are three type of basic MPPT technique namely P&O, tip speed ratio (TSR) and optimal relationship based (ORB). In Ref. [23], a modified MPPT for two stage PMSG based WECS is proposed for DC microgrid application. The MPPT is implemented using the grid side converter as boost converter. Further, P&O is the fundamental of all the machine side parameter independent MPPT technique. However, P&O has long convergence time for small perturbation and large oscillation with large perturbation. A comparative analysis of main MPPT technique is tabulated in Table 2.

It is of our interest to implement MPPT which is independent of machine parameter and wind speed for SEIG based WECS feeding DC nanogrid. In this paper the MPPT is implemented using the grid side converter (DC-DC converter) for a wide range of wind speed. Moreover, a simple control strategy for MPPT has been achieved with simple duty ratio control of DC-DC converter. Considering the ease of implementation, cost, accuracy and efficiency a modified P&O MPPT

**Table 1**
Comparison of various wind generator topologies.

| | SCIG | WRIG | DFIG | PMSG | WRSG |
|---|---|---|---|---|---|
| Operating speed range | 0–100% | ± 10% | ± 30% | 0–100% | 0–100% |
| Converter rating | 100% | 10% | 30% | 100% | 100% |
| MPPT | Possible | Partially Possible | Possible | Possible | Possible |
| Soft starter | Not Required | Required | Not Required | Not Required | Not Required |
| Cost | Very Low | Moderate | Moderate | High | High |
| Efficiency | High | Low | High | High | High |
| Maintenance | Very low | Moderate | Moderate | High | High |
| DC nanogrid integration | Simple | Complex | Complex | Simple | Moderate |
| Reactive power compensation | Grid/Capacitor bank | Grid | Grid | Grid | NA |
| Technology | Emerging | Outdated | Matured | Matured | Matured |

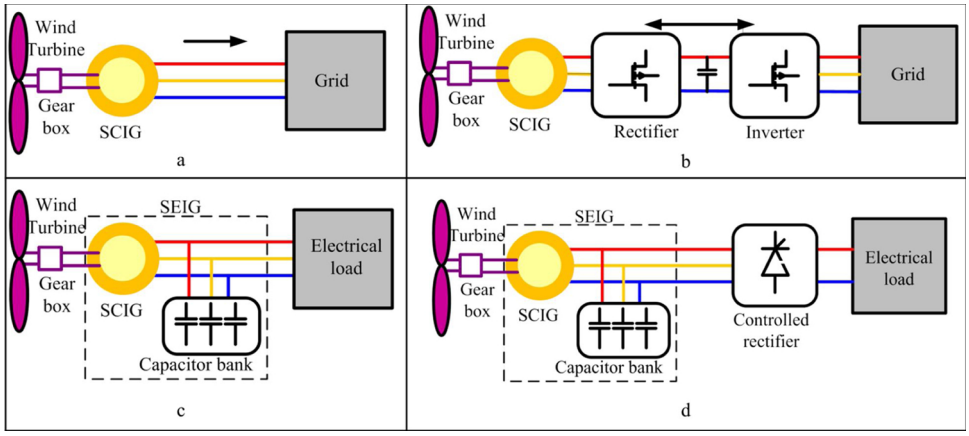


**Fig. 1.** Different topology of SEIG based WECS.

**Table 2**
Comparative analysis of MPPT techniques.

| | P&O | TSR | ORB | Proposed |
|---|---|---|---|---|
| No. of sensor | 02(V&I) | 03(V,I&A) | 02(V&I) | 01(I) |
| Knowledge of system parameter | No | Yes | Yes | No |
| Convergence speed | Slow | Fast | Fast | Moderate |
| Oscillation | Yes | No | No | Yes |
| Adaptive | Yes | No | No | Yes |
| Memory requirement | Low | Low | High | Low |
| Complexity | Simple | Simple | Complex | Complex |
| Cost | Low | High | Moderate | Low |

technique has been used for extracting maximum power in the present work. In the proposed technique MPPT is done by maximizing the DC grid current by varying the duty cycle of the DC-DC converter. The proposed MPPT has been implemented using different DC-DC converters, and at different DC grid voltage ratings.

This paper presents a comprehensive comparative analysis of proposed SEIG with DBR based WECS with previously proposed SEIG topologies in the literature based on the harmonic spectrum analysis. In contrast to conventional SEIG based WECS topologies having six controllable switches in rectifier, the proposed DC nanogrid has one controllable switch which simplifies the control strategy of SEIG and

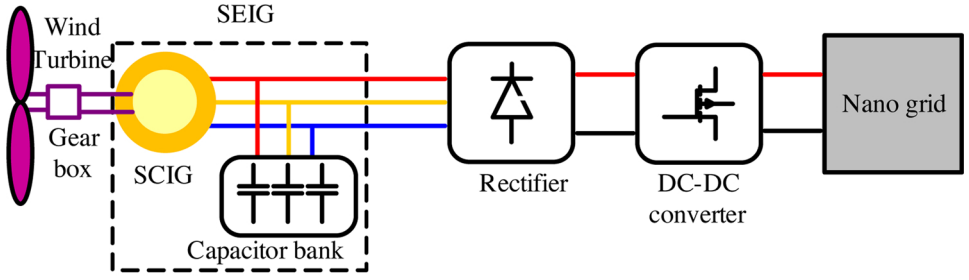


(a)

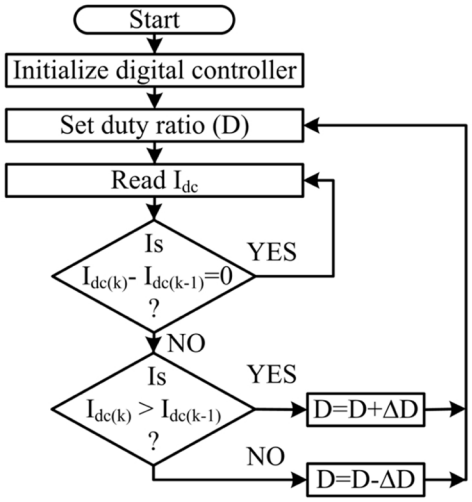


(b)

**Fig. 2.** Proposed wind driven SEIG (a) System architecture (b) MPPT algorithm.

reduces the cost. Further, the use of DBR enhances the efficiency of the SEIG by reducing the harmonic injection on the machine side. DC-DC converter is employed to implement MPPT technique at the output of the DBR and also performs the role of voltage regulator when SEIG based WECS employed in the stand-alone mode. The use of a DC-DC converter gives an added advantage of selective harmonic elimination switching, resulting reduced losses and simple control. Further, a single sensor, simple, cost effective and modified P&O MPPT is implemented for analysis of SEIG based DC nanogrid. Further, the impact of the selection of non- isolated DC-DC converter for implementing MPPT in the proposed topology of WECS for DC nanogrid through detailed simulation and experiments under various dynamic conditions is analyzed. Different types of non-isolated DC-DC converters (buck, boost, cuk) have been used for analyzing the MPPT and dynamic performance of the WECS at different DC grid voltage conditions. The entire system has been modeled and simulated in MATLAB/simulink. In the following sections of the paper, system description, mathematical modelling, DBR based topology harmonic spectrum analysis, dynamic performance of the system under grid connected mode of operation with different converters has been illustrated in detail.

## 2. System architecture

A DC nanogrid topology consisting of SCIG with delta connected capacitor bank forming a SEIG coupled to variable wind turbine is connected to a combination of DBR and DC-DC converter is proposed in this paper. The schematic of the WECS is shown in Fig. 2(a). The reactive power requirement of the SCIG is met by the capacitor bank connected in parallel to the generator. The combination of DBR and DC-DC converter is used in the proposed topology has replaced the controlled/semi-controlled rectifier in the conventional nanogrid topology. In contrast to conventional SEIG based WECS topologies having six controllable switches in rectifier, the proposed DC nanogrid has one controllable switch which simplifies the control strategy of SEIG and reduces the cost. Further, the use of DBR enhances the efficiency of the SEIG by reducing the harmonic injection on the machine side. DC-DC converter is employed to implement MPPT technique at the output of the DBR and also performs the role of voltage regulator when SEIG based WECS employed in the stand-alone mode. The use of a DC-DC converter gives an added advantage of selective harmonic elimination switching, resulting reduced losses and simple control. As different types of DC-DC converter such as buck converter, boost converter and cuk converter are available, therefore, the right selection of the DC-DC converter for SEIG based DC nanogrid application is essential. Thus, detailed performance analysis of the proposed DC nanogrid topology consisting the combination of DBR with different types of DC-DC converter is a prerequisite and carried out in this work. A simple and easy to implement modified P&O MPPT technique as shown in Fig. 2(b) has been implemented in this study. Different types of non-isolated DC-DC converters (buck, boost, cuk) have been used for analyzing the MPPT and dynamic performance of the WECS at different DC grid voltage conditions. Considering the factors as safety, efficiency and cost, in this study grid voltage of 120 V and 380 V DC has been considered to analyze the wide range operation of DC-DC converters [24].

## 3. Modelling of the WECS

The WECS under study employs a 3.7 kW, 230 V, 3 phase, 4 pole, 50 Hz, delta connected SCIG, three phase DBR and DC-DC converter. The modelling equation of the system used for modelling is discussed in the following section of the paper.

### 3.1. Mathematical modelling of wind turbine

Following mathematical equation has been used for the modelling of the wind turbine in Matlab/simulink. The mechanical power of the wind ($P_w$) is given by Eq. (1) where, ρ is air density, R is radius of the turbine, $C_p$ is turbine power coefficient, and $V_w$ is wind velocity.

$$P_w = \frac{1}{2} C_p(\lambda, \theta)\rho\pi R_t^2 V_w^3 \tag{1}$$

$T_L$ and $T_m$ are mechanical and load torque, whereas λ is tip speed ratio.

$$T_L = \frac{P_w}{\omega_t} \tag{2}$$

$$T_m = \frac{T_t}{\xi} \tag{3}$$

$$\lambda = \frac{\omega_t R_t}{V_w} \tag{4}$$

The power coefficient $C_p(\lambda, \theta)$ is estimated by:

$$C_p(\lambda, \theta) = 0.22\left(\frac{116}{\lambda_i} - 0.4\theta - 5\right)e^{-12.5/\lambda_i} \tag{5}$$

$$\frac{1}{\lambda_i} = \frac{1}{\lambda + 0.08\theta} - \frac{0.035}{1 + \theta^3} \tag{6}$$

### 3.2. Modelling of the SCIG

The dynamic rotor and stator currents equation with respect to the stator flux coordinates of the generator is given by:

$$L_s \frac{d}{dt}(i_{sq}) = v_{sq} - R_s i_{sq} - (\omega_{ms})(L_s i_{sd} + L_o i_{rd}) - L_o \frac{d}{dt}(i_{rq}) \tag{7}$$

$$L_s \frac{d}{dt}(i_{sd}) = v_{sd} - R_s i_{sd} + (\omega_{ms})(L_s i_{sq} + L_O i_{rq}) - L_o \frac{d}{dt}(i_{rd}) \tag{8}$$

$$L_r \frac{d}{dt}(i_{rq}) = v_{rq} - R_r i_{rq} + (\omega_{ms} - \omega_e)(L_r i_{rd} + L_o i_{sd}) - L_o \frac{d}{dt}(i_{sq}) \tag{9}$$

$$L_r \frac{d}{dt}(i_{rd}) = v_{rd} - R_r i_{rd} + (\omega_{ms} - \omega_e)(L_r i_{rq} + L_o i_{sq}) - L_o \frac{d}{dt}(i_{sd}) \tag{10}$$

### 3.3. Modelling of the excitation system

The state equation of the fixed excitation capacitor bank has been derived using the d-q components of stator voltage as state variable, and is given by:

$$\frac{d}{dt}(v_{sd}) = 1/C(i_{sd} - i_{ld} + i_d) + \omega_{ms} v_{sq} \tag{11}$$

$$\frac{d}{dt}(v_{sq}) = 1/C(i_{sq} - i_{lq} + i_q) + \omega_{ms} v_{sd} \tag{12}$$

### 3.4. Modelling of the converters

A DC-DC converter has two mode of operation. Eqs. (13) and (14) shows the mode of operation when switch is ON. The second mode of operation i.e. switch is OFF is given by Eqs. (13) and (15). The modelling equation of buck converter is given by:

$$\frac{d}{dt}(V_c) = \frac{i_L}{C} - \frac{V_c}{R_c} \tag{13}$$

$$\frac{d}{dt}(i_L) = \frac{V_{in}}{L} - \frac{V_c}{L} \tag{14}$$

$$\frac{d}{dt}(i_L) = -\frac{V_c}{L} \tag{15}$$

Boost converter modelling equation is given by Eqs. (13)–(17). Eqs. (16) and (17) represent boost converter when switch is ON and Eqs.

(13) and (14) when switch is OFF.

$$\frac{d}{dt}(i_L) = \frac{V_{in}}{L} \tag{16}$$

$$\frac{d}{dt}(V_c) = -\frac{V_c}{R_c} \tag{17}$$

The modelling equation of cuk converter is given by:

$$\frac{d}{dt}(i_L) = \frac{V_{in}}{L} - \frac{(1-D)V_c}{L} \tag{18}$$

$$\frac{d}{dt}(i_{Lo}) = \frac{DV_c}{L_o} - \frac{V_{co}}{L_o} \tag{19}$$

$$\frac{d}{dt}(V_c) = \frac{(1-D)i_L}{C} - \frac{Di_{Lo}}{C} \tag{20}$$

$$\frac{d}{dt}(V_{co}) = \frac{i_{Lo}}{C_o} - \frac{V_{co}}{RC_o} \tag{21}$$

## 4. Performance analysis of proposed DC nanogrid topology

Conventionally, SEIG based WECS topology consists of controlled/semi-controlled rectifier. However, a combination of DBR and DC-DC converter has been proposed in this study to employ the SEIG as micro-source for DC nanogrid. The performance of the proposed DC nanogrid topology is analyzed through simulations. Also, the hardware prototype of the proposed system shown in Fig. 3 is developed to validate the selection of DBR and DC-DC converter for SEIG. The laboratory scale prototype of the system consists of 3.7 kW, 230 V, 3 phase, 4 pole, 50 Hz, delta connected SCIG with capacitor bank rated 100 uf per phase forms the SEIG is connected to three phase DBR and cuk converter which supplies the load. The machine parameter obtained are $R_1 = 1.3\,\Omega$, $R_2 = 1.78\,\Omega$, $X_1 = X_2 = 2.56\,\Omega$. The DC-DC converters design equations used for calculation are given in Appendix A. Based on voltage and current withstand capability and switching frequency the selection of semiconductor switches is done. Since, the switching frequency in the present work is 25 kHz and current is less than 20A. MOSFET IRFP460 is used as switch in DC-DC converter. A MOSFET can operate at frequency up to 100 kHz but has less voltage and current rating as compared to IGBT. A 3-phase DBR based module VS-36MT160 was used for rectifying the generator output to DC. A gate driver circuit using IC TLP250 was designed for amplifying the gate pulse generated from microcontroller and provide isolation between control and power circuit. ST-Microelectronics make STM32F407VGT6 a 32 bit micro controller unit of STM32F4 family and commonly known as digital signal controller is used as controller in this work.

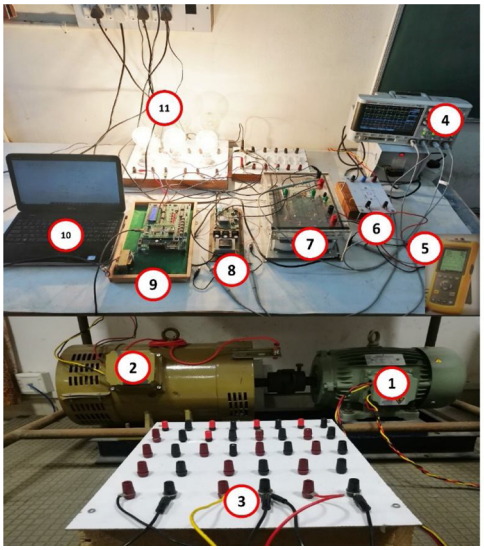


**Fig. 3.** Prototype hardware setup to demonstrate the performance of DC nanogrid.

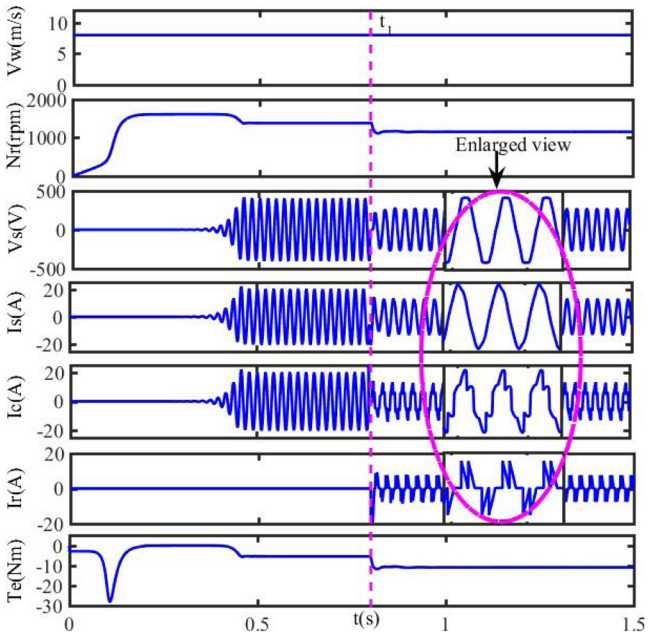


(a)

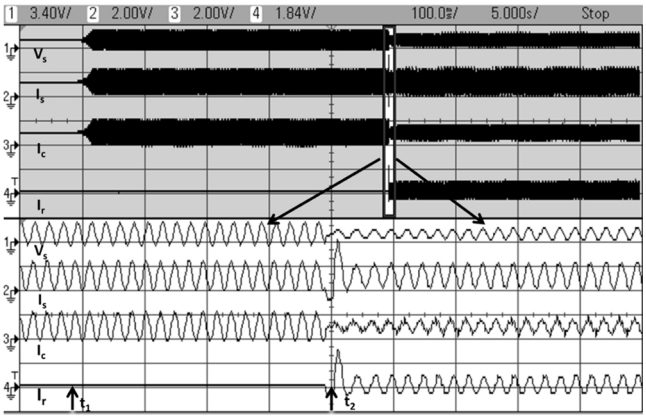


(b)

**Fig. 4.** Voltage buildup during self-excitation and operation of converters (a) simulation (b) experimental.
Scale: channel1 = 500 V/div, channel2 = 20A/div, channel3 = 20A/div, channel4 = 20A/div.

### 4.1. Comparative analysis of DC nanogrid topology using DBR and semi-controlled rectifier

The controlled/semi-controlled rectifier in the conventional topology is replaced by combination of DBR with DC-DC converter in the proposed WECS based DC nanogrid topology. In conventional DC nanogrid topology, the rectifier has 6 controllable power switches and each requires the control signal. Whereas, in proposed topology, combination of DBR with DC-DC converter has only one controllable switch which would simplify the control and reduces the cost of the power electronic control for SEIG. Further, the simulation results for voltage buildup during self-excitation and initiation of converter operation at is shown in Fig. 4(a). The Fig. 4(b) shows the experimentally obtained

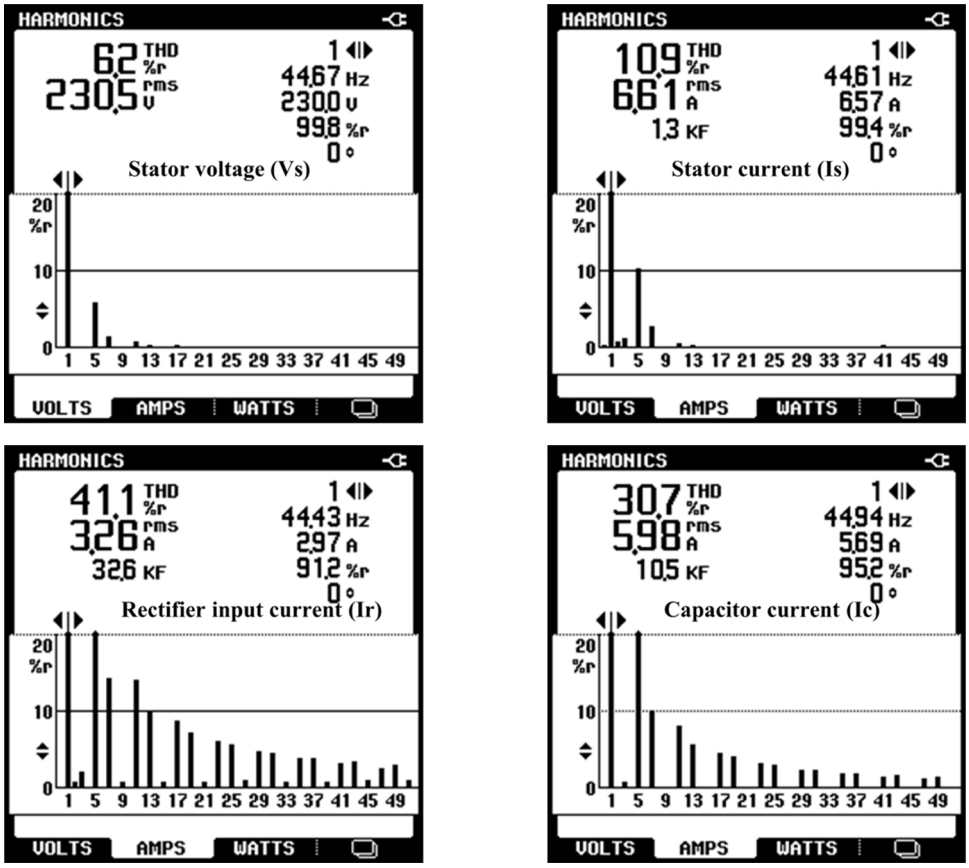


**Fig. 5.** Harmonic spectrum of an SEIG based WECS.

digital storage oscilloscope (DSO) waveforms of stator line voltage ($V_s$), stator line current ($I_s$), capacitor line current ($I_c$) and input line current ($I_r$) to the rectifier. Then, the harmonic spectrum analysis of an SEIG-converter system is done to analyze the performance of the DBR in SEIG based topology. The harmonic spectrum analysis results obtained experimentally for proposed topology are shown in Fig. 5. The total harmonic distortion (THD) in $V_s$, $I_s$, $I_r$, and $I_s$ are 6.2%, 10.9%, 41.1%, 30.7% respectively. Whereas, the THD in $V_s$, $I_s$, $I_r$, and $I_s$ for the semi-controlled rectifier based SEIG topology in [22] are 9.3%, 25.9%, 76.3% and 31.2% respectively.

The harmonic spectrum analysis depicts that the THD in the stator current and voltages has reduced due to the use of DBR in place of controlled/semi-controlled rectifier in proposed SEIG based DC nanogrid topology. Hence, the machine losses due to the presence of harmonics are reduced which enhances the efficiency of the SEIG based topology.

### *4.2. Performance analysis of DC nanogrid topology using DBR with different DC-DC converters*

In the proposed DC nanogrid topology, the DBR has enhanced the efficiency of the system reducing the harmonics in the machine as compared to the semi-controller rectifier based SEIG topology. As, the DBR is used in combination with the DC-DC converter to implement the MPPT algorithm in grid connected mode or voltage regulation in the stand-alone mode of the SEIG topology. Thus, it would be interesting to analyze the performance of the proposed system to perform comprehensive harmonic spectrum analysis with different DC-DC converter. The simulations are carried out for different DC-DC converter at same operating condition in combination with DBR connected to the SEIG driven by wind turbine and supplying the resistive load. The THD in $V_s$, $I_s$, $I_r$, and $I_s$ for buck converter, boost converter and cuk converter in the proposed DC nanogrid topology are shown in Fig. 6 and summarized in Table 3. It is observed from the Table 3 that the cuk converter has least THD among the three converters for the proposed DC nanogrid topology.

### *4.3. Dynamic performance analysis of DC nanogrid topology for MPPT using different DC-DC converters*

To validate the satisfactory dynamic performance of the proposed system with the MPPT controller, simulation has been carried out for step change in wind velocity. In this simulation, wind velocity has been changed from 8 m/s to 10 m/s and vice-versa. The simulated waveforms of rotor speed ($N_r$), electromagnetic torque ($T_e$) of generator, stator output power ($P_g$), $V_s$, $I_s$, $I_c$ and $I_r$ along with the DC grid current ($I_{dc}$), voltage ($V_{dc}$) and power ($P_{dc}$) have been observed for the step change in wind velocity ($V_w$). Fig. 7 shows the dynamic performance of buck converter based SEIG system. At time ($t_1$ = 1 s) the input wind velocity has been changed to 10 m/s from 8 m/s and vice versa at $t_2$ = 1.5 s. The

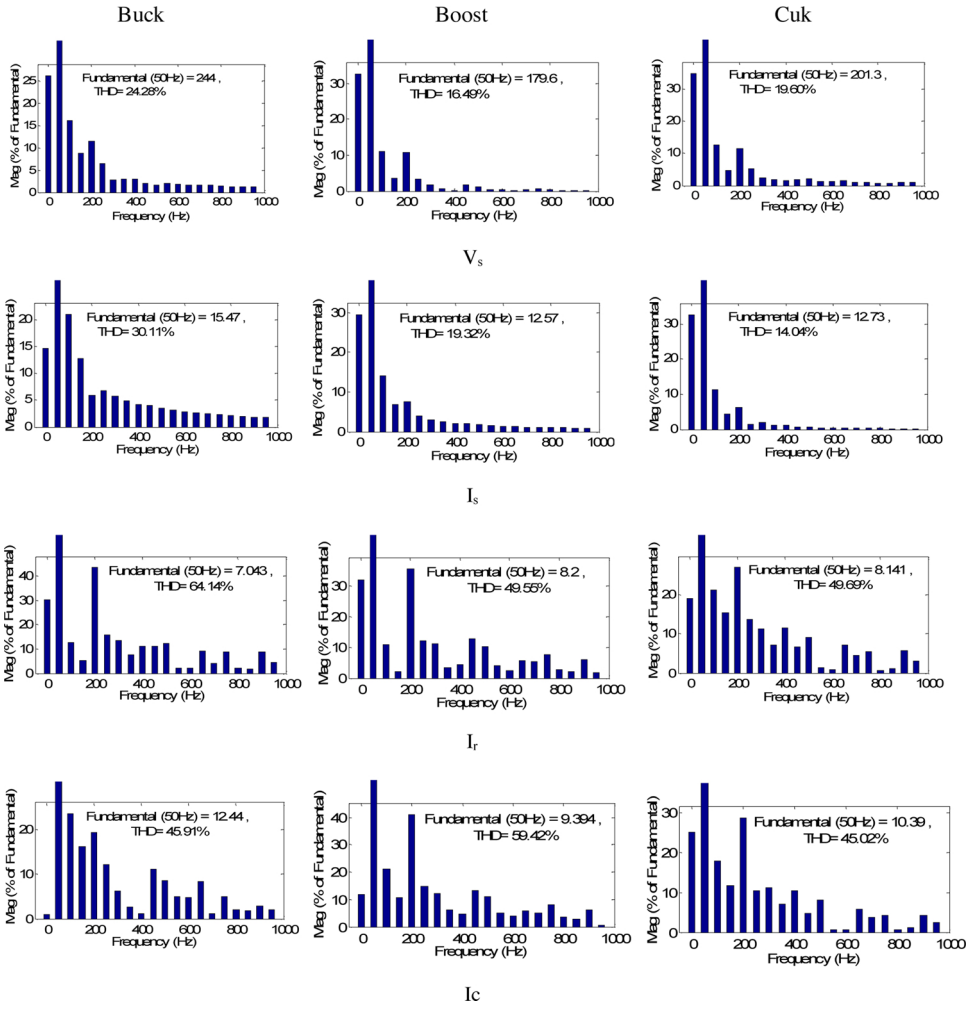


**Fig. 6.** Harmonic spectrum of an SEIG based WECS for different converetrs.

**Table 3**
Harmonic spectrum analysis for the different DC-DC converters in the proposed DC nanogrid.

| Converter/THD | $V_s$ | $I_s$ | $I_r$ | $I_c$ |
|---|---|---|---|---|
| Buck converter | 24.28% | 30.11% | 64.14% | 45.91% |
| Boost converter | 16.49% | 19.32% | 49.55% | 59.42% |
| Cuk converter | 19.60% | 14.04% | 49.69% | 45.02% |

corresponding change in $N_r$, $V_s$, $I_s$, $I_c$, $I_r$, $P_g$, $T_e$, $V_{dc}$, $I_{dc}$, $P_{dc}$ is shown in Fig. 7. It can be perceived from this figure that the $I_{dc}$ at 8 m/s and 10 m/s are 7.72A and 16.27A respectively. The MPPT technique is able to track the maximum power. The maximum power at 8 m/s and 10 m/s are 952 W and 2033 W respectively. The maximum overshoot in current is in the allowable limit. The above results show the satisfactory working of MPPT technique. Further, the simulation has been carried out with boost converter based SEIG system for grid voltage of 380 V. Fig. 8 shows the dynamic performance of boost converter based SEIG system for step change in wind velocity from 8 m/s to 10 m/s. The maximum power at 8 m/s and 10 m/s are 1031 W and 1914 W respectively.

Finally, the simulation was carried out for cuk converter based SEIG system and the results are shown in Fig. 9. Since, a nanogrid may operate at different voltage level. The grid voltage is changed from 380 V to 120 V, and the system dynamic performance is evaluated. When buck converter is employed for MPPT with the grid voltage of 380 V, the converter fails to operate because the required voltage gain is more than 1. Similarly, when the grid voltage is 120 V the boost converter is not able to supply at 120 V. Thus, a cuk converter is employed to meet the wide range of operation. Fig. 9(a) shows the dynamic performance of cuk converter based SEIG system for step change in grid voltage from 380 V to 120 V. The corresponding change in $N_r$, Vs, $I_s$, $I_c$, $I_r$, $P_g$, $T_e$, $V_{dc}$, $I_{dc}$, $P_{dc}$ is shown in Fig. 9(a). It can be observed from this figure that the $I_{dc}$ at 380 V and 120 V grid voltage are 5.1A and 16.05A respectively. The MPPT technique is able to track the maximum power at different DC grid voltages. The maximum power at 380 V and 120 V grid voltage is 1935 W and 1958 W respectively. Further step change in wind velocity for 380 V and 120 V system was simulated and the corresponding results are shown in Fig. 9(b) and (c). From the above analysis, it can be

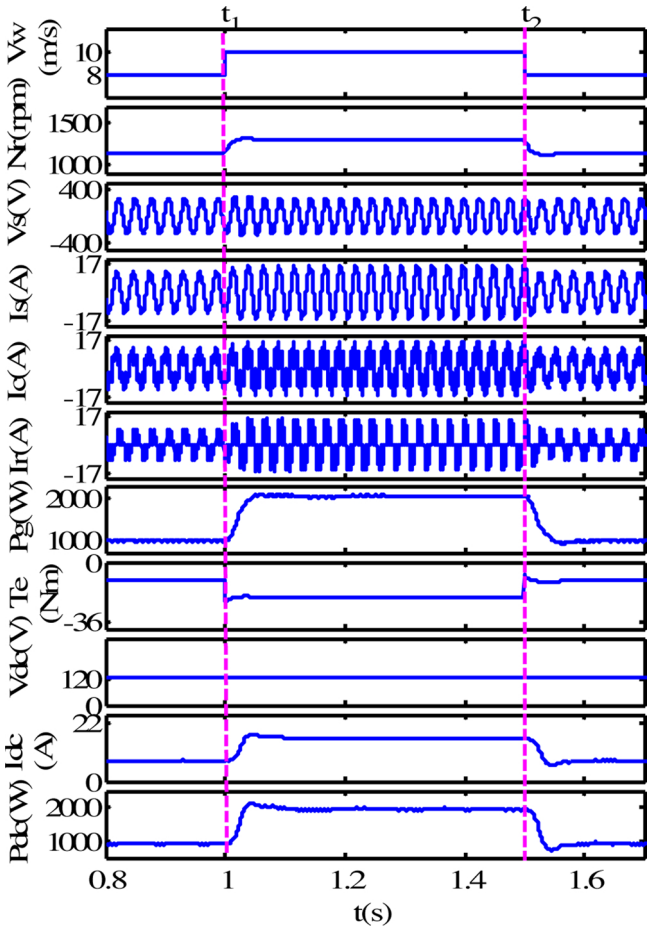


**Fig. 7.** Dynamic performance of buck converter based WECS for step change in wind speed from 8 m/s to 10 m/s and back.

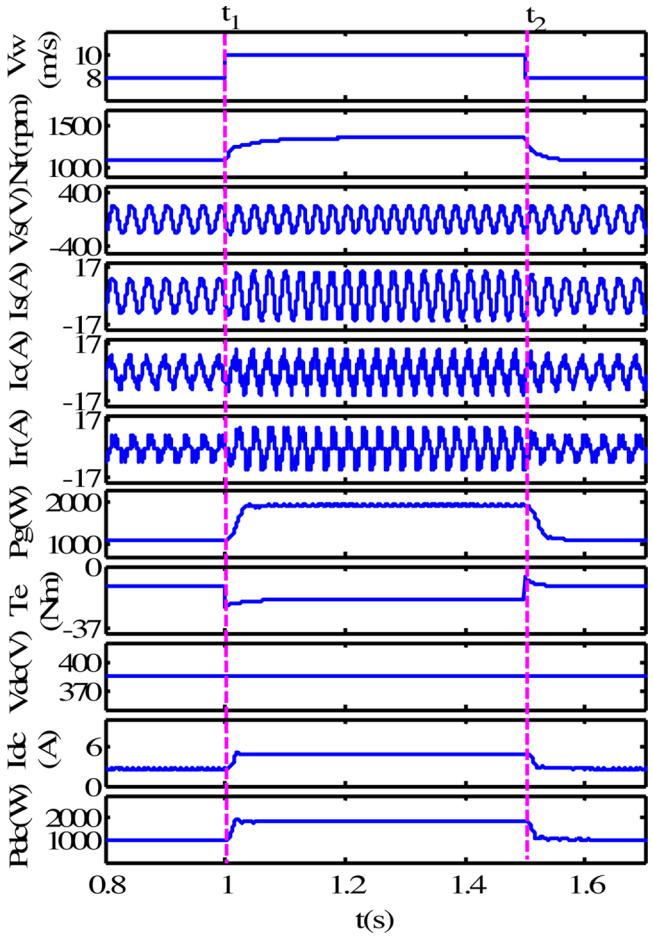


**Fig. 8.** Dynamic performance of boost converter based WECS for step change in wind speed from 8 m/s to 10 m/s and back.

concluded that the same MPPT algorithm is able to track MPP efficiently with all the converters. However, with cuk converter, we are able to achieve wide range of operation without any change in algorithm and hardware. Also, the efficiency curve as function of the power is shown in Fig. 10, suggests that cuk converter has higher efficiency than boost converter. A comparison of the proposed topology with the existing topology in the literature based on various parameters is carried out and tabulated in Table 4.

## 5. Conclusion

A SEIG based DC nanogrid topology consisting of a combination of DBR with DC-DC converter is proposed in this paper which has replaced the controlled/semi-controller rectifier of the conventional SEIG based topology. The choice of the DBR in the proposed topology has reduced the number of controllable switches from six as in the conventional topology to one. It clearly indicates that the control strategy is simplified and cost effective in the proposed DBR based topology. Further, the comparative harmonic spectrum analysis justifies that the choice of DBR over the controlled/semi-controlled rectifier in the proposed topology enhances the SEIG efficiency by reducing the THD in stator current and voltage of the SEIG. The laboratory scale prototype is developed for the validation of DBR based SEIG topology. Further, the detailed analysis is carried for the selection of the DC-DC converter which is based on the two factors viz. the effect of the type of DC-DC converter on the harmonic injection on the machine side and dynamic performance of the system during MPPT mode. It is concluded from the extensive simulations that the cuk converter implementation with DBR has least THD in the SEIG current and voltage as compared with that of buck converter and boost converter. Further, the dynamic performance analysis of the proposed DC nanogrid is carried out for the MPPT mode for which modified P&O algorithm is implemented using different DC-DC converters (buck converter, boost converter and cuk converter). It is observed from the simulation results that the cuk converter provides the wide range of operation for MPPT and flexibility in choosing the grid voltage as it gives satisfactory performance for both 120 V and 380 V grid voltages due to its voltage step up and down operation.

## Conflict of interest

None.

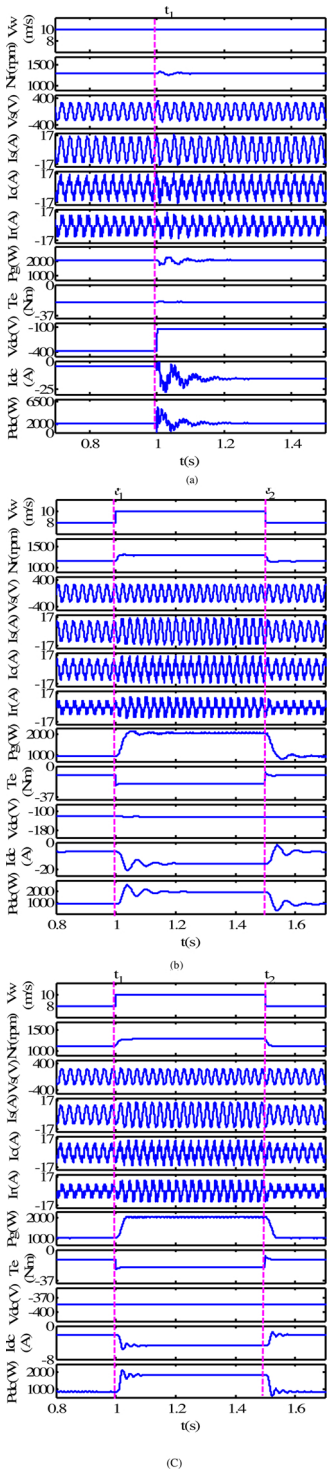


**Fig. 9.** Dynamic performance of cuk converter based WECS for (a) change in grid voltage from 380 to 120 V (b) step change in wind speed from 8 m/s to 10 m/s and back when the grid voltage is 120 V (c) Step change in wind speed from 8 m/s to 10 m/s and back when the grid voltage is 380 V.

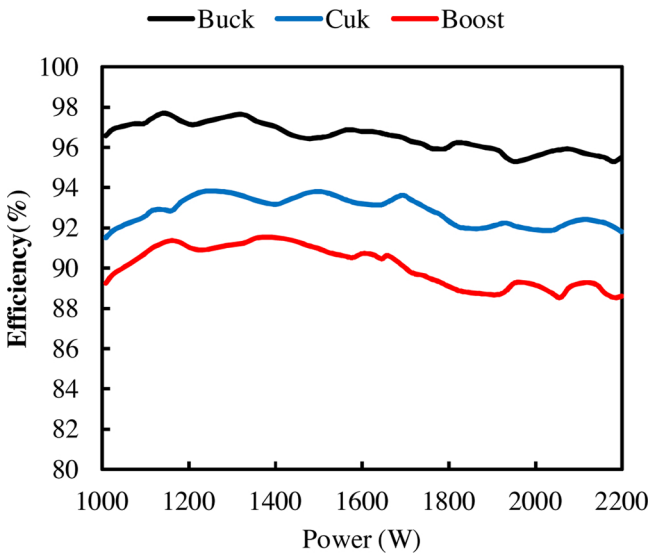


**Fig. 10.** Efficiency curve for buck, cuk and boost converter.

**Table 4**
Comparison of various topology of SEIG based WECS.

| | Single stage controlled rectifier | Single stage semi controlled rectifier | Two stage with DBR and DC-DC converter |
|---|---|---|---|
| No. of Controllable switch | 06 | 03 | 01 |
| Switching device | Thyristor | Thyristor | MOSFET/IGBT |
| THD | High | High | Low |
| Conduction losses | High | High | Low |
| MPPT | Possible | Possible | Possible |
| Reliability | Low | Low | High |
| Control complexity | Complex | Moderate | Simple |
| Displacement factor | < 1 | < 1 | 1 |
| Efficiency | Low | Low | High |

## CRediT authorship contribution statement

**Saurabh Kumar:** Conceptualization, Methodology, Software, Visualization, Investigation, Writing - original draft. **Vijayakumar K:** Supervision, Software, Validation, Funding acquisition, Writing - review & editing.

## Acknowledgments

This work was supported and funded by Science and Engineering Research Board (SERB), Department of Science and Technology (DST), in the department of electronics and communication engineering, Indian Institute of Technology and Design Kancheepuram, Chennai under the project reference number YSS/2015/001473.

## Appendix A

Following equations has been used for design of converters parameters:
Buck converter design equation

$$D = \frac{V_o}{V_s},\ L_{\min} = \frac{(1-D)R}{2f},\ C = \frac{1-D}{8L\frac{\Delta V_o}{V_o}f^2}$$

Boost converter design equation

$$D = 1 - \frac{V_s}{V_o},\ L_{\min} = \frac{D(1-D)^2R}{2f},\ C = \frac{D}{R\frac{\Delta V_o}{V_o}f}$$

Cuk converter design equation

$$D = \frac{V_o}{V_o - V_s},\ L_1 \geq \frac{V_s D}{f\Delta i_{L1}},\ L_2 \geq \frac{V_s D}{f\Delta i_{L2}}$$

Where, $\Delta i_L = \frac{V_s D}{Lf}$

$$C_1 \geq \frac{V_o D}{Rf\Delta v_{C1}},\ C_2 \geq \frac{1-D}{8L_2\frac{\Delta V_o}{V_o}f^2}$$

## Appendix B. Supplementary data

Supplementary data associated with this article can be found, in the online version, at https://doi.org/10.1016/j.epsr.2020.106196.

## References


[1] Global Energy Statistical Yearbook, (2018) (n.d.).
[2] The Outlook for Energy: A view to 2040, ExxonMobil, Texas, United States, 2013.
[3] F. Shahnia, A. Ghosh, R.P.S. Chandrasena, S. Rajakaruna, Dynamic operation and control of a hybrid nanogrid system for future community houses, IET Gener. Transm. Distrib. 9 (2015) 1168–1178, https://doi.org/10.1049/iet-gtd.2014.0462.
[4] O. Lucia, I. Cvetkovic, H. Sarnago, D. Boroyevich, P. Mattavelli, F.C. Lee, Design of home appliances for a DC-based nanogrid system: an induction range study case, IEEE J. Emerg. Sel. Top. Power Electron 1 (4) (2013) 315–326.
[5] W. Wu, H. Wang, Y. Liu, M. Huang, F. Blaabjerg, A dual-buck-boost AC/DC converter for DC nanogrid with three terminal outputs, IEEE Trans. Ind. Electron. 64 (2017) 295–299, https://doi.org/10.1109/TIE.2016.2598804.
[6] M. Nasir, H.A. Khan, A. Hussain, L. Mateen, N.A. Zaffar, Solar PV based scalable DC microgrid for rural electrification in developing regions, IEEE Trans. Sustain. Energy. 9 (2018) 390–399, https://doi.org/10.1109/TSTE.2017.2736160.
[7] B. Wang, L. Xian, U. Manandhar, J. Ye, X. Zhang, H.B. Gooi, A. Ukil, Hybrid energy storage system using bidirectional single-inductor multiple-port converter with model predictive control in DC microgrids, Electr. Power Syst. Res. 173 (2019) 38–47, https://doi.org/10.1016/j.epsr.2019.03.015.
[8] M. Shahidehpour, Z. Li, W. Gong, S. Bahramirad, M. Lopata, A hybrid AC/DC nanogrid: the Keating Hall installation at the Illinois Institute of Technology, IEEE Electrif. Mag. (2017) 36–46.
[9] V. Nayanar, N. Kumaresan, N.G. Ammasai Gounden, Wind-driven SEIG supplying DC microgrid through a single-stage power converter, Eng. Sci. Technol. Int. J. 19 (2016) 1600–1607, https://doi.org/10.1016/j.jestch.2016.05.016.
[10] D.N. Gaonkar, P. Jayalakshmi, N.S. Raghvendra, Performance study of roof top wind solar microgrid system in isolated mode of operation, Power Electron. Drives Energy Syst. (2014) 1–6.
[11] K. Vijayakumar, N. Kumaresan, N.A. Gounden, Operation and closed-loop control of wind-driven stand-alone doubly fed induction generators using a single inverter-battery system, IET Electr. Power Appl. 6 (2012) 162–171.
[12] K. Vijayakumar, N. Kumaresan, N.G. Ammasai Gounden, Speed sensor-less maximum power point tracking and constant output power operation of wind-driven wound rotor induction generators, IET Power Electron. 8 (2015) 33–46, https://doi.org/10.1049/iet-pel.2013.0700.
[13] V. Yaramasu, A. Dekka, M.J. Durán, S. Kouro, B. Wu, PMSG-based wind energy conversion systems: survey on power converters and controls, IET Electr. Power Appl. 11 (2017) 956–968.
[14] X. Zhang, Y. Zhang, S. Hao, L. Wu, W. Wei, An improved maximum power point tracking method based on decreasing torque gain for large scale wind turbines at low wind sites, Electr. Power Syst. Res. 176 (2019) 105942, , https://doi.org/10.1016/j.epsr.2019.105942.
[15] G.K. Singh, Self-excited induction generator research - a survey, Electr. Power Syst. Res. 69 (2004) 107–114, https://doi.org/10.1016/j.epsr.2003.08.004.
[16] H. Li, Z. Chen, Overview of different wind generator systems and their comparisons, Renew. Power Gener. IET. 2 (2008) 123–138, https://doi.org/10.1049/iet-rpg:20070044.
[17] R.C. Bansal, Three-phase self-excited induction generators: an overview, IEEE Trans. Energy Convers. 20 (2005) 292–299, https://doi.org/10.1109/TEC.2004.842395.
[18] R.C. Bansal, T.S. Bhatti, D.P. Kothari, Bibliography on the application of induction generators in nonconventional energy systems, IEEE Trans. Energy Convers. 18 (2003) 433–439, https://doi.org/10.1109/TEC.2003.815856.
[19] F. Jiang, C. Tu, Z. Shuai, F. Xiao, Z. Lan, Combinational voltage booster technique for fault ride-through capability enhancement of squirrel-cage induction generator, Electr. Power Syst. Res. 136 (2016) 163–172, https://doi.org/10.1016/j.epsr.2016.02.010.
[20] L. Krichen, B. Francois, A. Ouali, A fuzzy logic supervisor for active and reactive power control of a fixed speed wind energy conversion system, Electr. Power Syst. Res. 78 (2008) 418–424, https://doi.org/10.1016/j.epsr.2007.03.010.
[21] D. Chermiti, N. Abid, A. Khedher, Voltage regulation approach to a self-excited induction generator: theoretical study and experimental validation, Int. Trans. Electr. Energy Syst. 27 (2017) e2311, https://doi.org/10.1002/etep.2311.
[22] R. Karthigaivel, N. Kumaresan, M. Subbiah, Analysis and control of self-excited induction generator-converter systems for battery charging applications, IET Electr. Power Appl. 5 (2011) 247–257, https://doi.org/10.1049/iet-epa.2010.0088.
[23] J. Chen, T. Lin, C. Wen, Y. Song, Design of a unified power controller for variable-speed fixed-pitch wind energy conversion system, IEEE Trans. Ind. Electron. 63 (2016) 4899–4908, https://doi.org/10.1109/TIE.2016.2547365.
[24] S. Anand, B.G. Fernandes, Optimal voltage level for DC microgrids, IECON Proceedings (Industrial Electronics Conference) (2010) 3034–3039, https://doi.org/10.1109/IECON.2010.5674947.